CORA Cork Open Research Archive
Cartlann Taighde Oscailte Chorcaí

Title	Thermal diffusivity of nonfractal and fractal nickel nanowires
Authors	Razeeb, Kafil M.;Roy, Saibal
Publication date	2008-04-21
Original Citation	Razeeb, K. M. and Roy, S. (2008) 'Thermal diffusivity of nonfractal and fractal nickel nanowires', Journal of Applied Physics, 103(8), pp. 084302. doi: 10.1063/1.2906347
Type of publication	Article (peer-reviewed)
Link to publisher's version	http://aip.scitation.org/doi/abs/10.1063/1.2906347 - 10.1063/1.2906347
Rights	© 2008 American Institute of Physics, This article may be downloaded for personal use only. Any other use requires prior permission of the author and AIP Publishing. The following article appeared in Razeeb, K. M. and Roy, S. (2008) 'Thermal diffusivity of nonfractal and fractal nickel nanowires', Journal of Applied Physics, 103(8), pp. 084302 and may be found at http://aip.scitation.org/doi/abs/10.1063/1.2906347
Download date	2026-11-01 03:05:17
Item downloaded from	https://hdl.handle.net/10468/4226

UCC
University College Cork, Ireland
Coláiste na hOllscoile Corcaigh

Thermal diffusivity of nonfractal and fractal nickel nanowires

Kafil M. Razeeb and Saibal Roy

Citation: Journal of Applied Physics **103**, 084302 (2008); doi: 10.1063/1.2906347
View online: http://dx.doi.org/10.1063/1.2906347
View Table of Contents: http://aip.scitation.org/toc/jap/103/8
Published by the American Institute of Physics



Thermal diffusivity of nonfractal and fractal nickel nanowires

Kafil M. Razeeb[a] and Saibal Roy
Tyndall National Institute, Lee Maltings, Prospect Row, Cork, Ireland

(Received 18 October 2007; accepted 14 February 2008; published online 21 April 2008)

The potential of using nanometallic wires inside a matrix as new generation of thermal interface material led us to study the thermal diffusivity of nickel nanowires embedded inside porous alumina template. Thermal diffusivity measurements using a laser flash method showed size dependence for nickel nanowires inside nanochannel alumina (NCA) templates having nominal pore diameters of 200, 100, and 20 nm. Nickel nanowires embedded inside these templates showed decreasing diffusivity values of 10.7×10^{-6}, 8.5×10^{-6}, and 6.5×10^{-6} $m^2\,s^{-1}$ at 300 K with decreasing wire diameter when deposited at 40 °C. Nanowires fabricated at 60 °C showed similar decreasing diffusivity with wire diameter, and a further 42%–48% reduction was observed when compared to 40 °C samples. The modified effective medium theory (MEMT) was employed to evaluate the experimental thermal diffusivity. Calculations based on MEMT resulted in mean thermal conductivities of 70.7 and 36.2 $W\,m^{-1}\,K^{-1}$ for nickel nanowires fabricated at 40 and 60 °C respectively. These values are ~20% and 60% lower than the thermal conductivity value of bulk nickel. A strong grain size dependence of thermal diffusivity in the nanowires was observed. It is believed that the decrease in diffusivity in lower temperature wires is associated with defects/dislocations in large single crystals and reduction in wire diameters according to pore diameters of NCA. Whereas in higher temperature wires, the drastic reduction in diffusivity is believed to arise from self-similar fractal morphology composed of nanogranules, close to the dimension of electron mean free path. © *2008 American Institute of Physics*. [DOI: 10.1063/1.2906347]

I. INTRODUCTION

One of the main limitations in power semiconductor device cooling is the microscopic unevenness and nonplanarity between the mating surfaces (chip and heat sink). Asperities on each of the surfaces prevent the two solids forming a thermally perfect contact.[1] Thermal interface materials are, therefore, used to provide a reliable heat conduction path between the two solid surfaces, which can conform to surface roughness. These are usually low cost conductive composites made of an insulating matrix loaded with micron sized conductive filler materials. Carbon nanotubes have recently been proposed as filler materials inside the polymer matrix to be used as thermal interface material because of their high thermal conductivity.[2–4] Metal nanowires and submicron wires can be a better choice because of their cost effective fabrication route compared to carbon nanotubes. These nanowires are high aspect ratio structures, so that an individual wire can make thermal contact across two surfaces, conforming micron scale unevenness of the mating surfaces. Nanowires made of nickel may be a good candidate, as nickel has good corrosion resistance and a low diffusion coefficient with other metals. Bulk nickel has room temperature thermal conductivity of 90.7 $W\,m^{-1}\,K^{-1}$ and diffusivity of 23×10^{-6} $m^2\,s^{-1}$. These nanowires can be easily fabricated by electrodeposition of nickel through the channels of prepatterned templates. Nanoporous membranes such as nanochannel alumina (NCA) are particularly suitable for the preparation of very high aspect ratio structures because the ratio of the length and diameter of the pores can be very large. However, the thermal properties and specifical thermal diffusivity of nickel nanowire or nickel-alumina composite are not yet reported, which are essential if these nanowires are to be used as filler materials in the thermal interface material system.

II. EXPERIMENTAL

The nickel nanowires were prepared inside the NCA template having three different pore diameters of 200, 100, and 20 nm on the filtration side. This side of the NCA was sputtered with 500 nm aluminum, acting as the metal substrate. Ohmic contact to the substrate was made by using Radionics silver conductive paint, which has a volume resistivity of 0.001 Ω cm when fully hardened. Nickel nanowires were fabricated by using galvanostatic electrodeposition technique by applying a constant current density of 10 $mA\,cm^{-2}$ using CHI660B potentiostat/galvanostat. The deposition was carried out until the pores were completely filled with nickel. The electrolyte was composed of 53.643 $g\,l^{-1}$ $NiSO_4\cdot6H_2O$ and 30 $g\,l^{-1}$ H_3BO_3. De-ionized water with resistivity of ~18 MΩ was used to prepare the solution. The *p*H of the solution was adjusted to 2.5 with addition of H_2SO_4 and stirred with a constant 660 rpm. The electrolyte temperature was maintained at 40 and 60 ± 0.2 °C to prepare two batch of samples and, henceforth, will be regarded as "low temperature" (40 °C) and "high temperature" (60 °C) samples. After deposition, the samples were thoroughly rinsed with de-ionized water and dried with nitrogen gun.

The pore filling of nickel was investigated by Hitachi S4000 scanning electron microscope (SEM). Transmission

[a]Electronic mail: kafil.mahmood@tyndall.ie.

 © 2008 American Institute of Physics

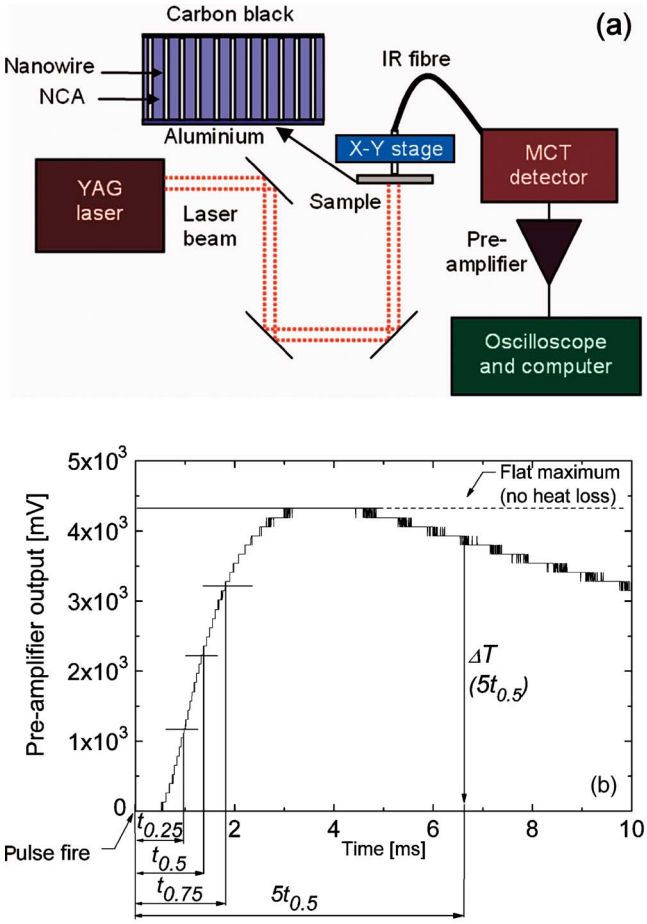


FIG. 1. (Color online) (a) Schematic of laser flash setup for the measurements of thermal diffusivity. (b) The shape of the thermal transient for nickel foil measured by the flash technique.

electron microscope (TEM) was used to study the nanostructure of the nickel wires. The cross section of the samples was prepared by focused ion beam (FIB) milling for TEM observation. The grain size distribution was obtained by counting and measuring the grain diameters from micrograph using IMAGEJ software. For further estimation of overall grain size and crystal orientation, x-ray diffraction (XRD) measurements were carried out by using a Philips PW3710 diffractometer with Cu $K\alpha_1$ radiation, having a wavelength of 1.540 56 Å.

Thermal diffusivity measurement of the nickel-alumina composites was carried out by using the laser flash method.[5,6] The flash method developed by Parker *et al.* is one of the most reliable methods for measuring thermal diffusivity in the direction perpendicular to the plane of relatively thin and planar samples.[7] The custom-built experimental setup is shown in Fig. 1(a), where a short laser pulse (using neodymium-doped yttrium aluminium garnet laser) with duration of 7 ns hit the samples to create an effectively instantaneous heat source. The substrate side (aluminum) was heated with the laser pulse where the diameter of the laser beam was 4 mm. An infrared detector was exactly positioned opposite to where the pulse impinges the sample for measurement of the thermal wave.

III. MEASUREMENT PRINCIPLE

The transient temperature on the detector side of the sample can be described as[8]

$$T(t) = \frac{E}{\rho c l}\left[1 + 2\sum_{n=1}^{\infty}(-1)^n \exp\left(\frac{-n^2\pi^2}{l^2}\alpha t\right)\right], \quad (1)$$

where E is the energy absorbed from the flash, ρ is the density of sample, c is the heat capacity, l is the sample thickness, and α is thermal diffusivity. A typical thermal transient curve obtained for pure Ni foil is shown in Fig. 1(b). The resulting rise in temperature was recorded by using the preamplifier and oscilloscope setup, controlled by using LABVIEW program. In this method, heat flow is assumed to be one dimensional in the direction perpendicular to the planar surfaces. The duration of the pulse is short enough to be considered effectively instantaneous in comparison with the time taken for the thermal transient to reach half of its maximum value. The time at which the curve reaches that value is given by the following equation:

$$t_{0.5} = \frac{1.38l^2}{\pi^2\alpha}, \quad (2)$$

where α is thermal diffusivity, l is thickness of the sample, and $t_{0.5}$ is the time at which the thermal curve reaches half of its maximum value at the opposite side of the sample. Diffusivity can be calculated by calculating the time $t_{0.5}$ in Fig. 1(b) and the thickness of the samples.

All the measurements were conducted in air and, therefore, heat loss correction was done for the radiative and convection heat losses according to Cowan, where an expression was derived for the temperature at the back face of a planar sample when there is a linear rate of heat loss from both faces of the sample.[9] The effect of these heat losses can be clearly seen in the plateau in Fig. 1(b). Here, the transient drops below its maximum level, whereas if there were no heat losses, the curve would remain completely flat. By using the relative height of the graph at the time at which it reaches half its maximum, $\Delta(t_{1/2})$, compared to the height of the graph at a later time, for example, at $5t_{1/2}$ or $10t_{1/2}$: $\Delta(10t_{0.5})/\Delta(t_{0.5})$, a corrected value was used instead of $1.38/\pi^2$ in Eq. (2). A graph was drawn showing the locus of $\alpha t_{0.5}/l^2$ for different values of $\Delta(10t_{0.5})/\Delta(t_{0.5})$, as shown in Fig. 2, according to Cowan. The other curve in Fig. 2 gives the change in $\alpha t_{0.5}/l^2$ for the relative height of the curve at five times the half maximum time—$\Delta(5t_{0.5})/\Delta(t_{0.5})$. Here, the ratio of heat losses at the front and back surfaces of the sample was considered to be equal. The corrected value of $\alpha t_{0.5}/l^2$ can be read from the graph by using the value of the transient at five times or ten times the half-time. The use of the latter part of the graph is very effective, as heat losses change in a very obvious and easily measurable way. If there were no heat losses, the value used was $1.38/\pi^2 = 0.138\,79$.

IV. MODEL

To compare the diffusivity values of nickel-alumina-composite samples having different nickel contents, modified effective medium theory[10] (MEMT) was used. It is assumed

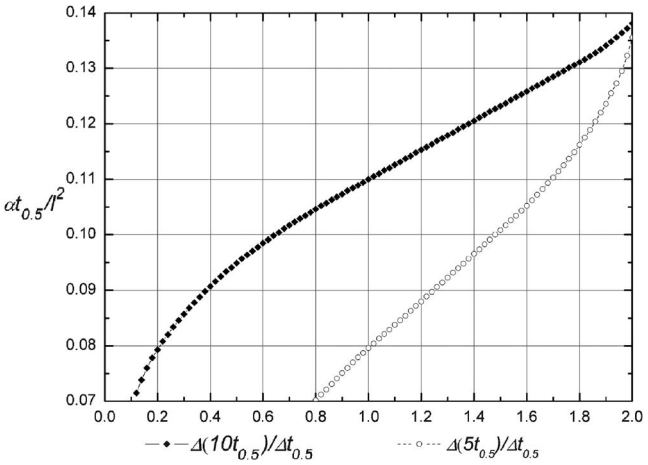


FIG. 2. Correction curves for heat losses using the relative amplitudes at ten and five times the half-time.

that high aspect ratio continuous fibers are uniformly distributed in the composite material, as shown in the schematic of Fig. 1(a). According to the rule of mixture for a simple parallel model, the effective thermal conductivity in the z direction is

$$k_z = k_m(1-\phi) + k_p\phi, \tag{3}$$

where k_z is the thermal conductivity of the composite material along the z direction (i.e., perpendicular to the sample surface), k_m and k_p are the bulk thermal conductivities of matrix and fiber, respectively, and ϕ is the percentage of fiber in the composite. To directly compare the experimental diffusivity data with the above model, Eq. (3) was reconfigured[11] to

$$\alpha = \frac{k_{\text{alumina}}(1-\phi) + k_{\text{Ni}}\phi}{(\rho c)_{\text{alumina}}(1-\phi) + (\rho c)_{\text{Ni}}\phi}, \tag{4}$$

where k is the thermal conductivity, (ρc) is heat capacity per unit volume for alumina and Ni, and ϕ is the percentage of Ni in the composite.

V. RESULTS AND DISCUSSION

A. Electron microscopy

Nickel nanowires fabricated inside NCA has different pore diameters. The average pore diameters were 310, 241, and 201 nm, which resulted in porosities of 50%, 40%, and 30% for NCA200, NCA100, and NCA20 templates, respectively.[12] Scanning electron microscopy analysis on top of the three templates revealed three different wire diameters according to the pore diameters of the templates. Figure 3(a) shows a representative SEM image of top of nickel nanowires fabricated at 40 °C inside NCA200 template. The nickel wires in NCA200 have an average diameter of 308 nm, which is comparable with the pore diameter on the reverse side. The density of the wires matched with the density of the pores, which is 10^8 cm^{-2}. Figure 3(b) shows the sample fabricated from 60 °C electrolyte where self-similar fractal growth can be observed in individual nanowire. The SEM image in Fig. 3(c) was taken after etching the Al seed layer with 10% NaOH solution. The micrograph at Fig. 3(d) shows aligned nanowires after completely removing NCA template. SEM observation on different areas of the electrodeposited templates confirmed that nearly 95% pores of the NCA were filled with nickel. Hence, the Ni content in each NCA samples was considered to be similar to the porosity value of that template.

TEM analysis revealed a wide range of grain size in nickel nanowires. Figure 4(a) shows the dark field image of low temperature sample with corresponding selected area diffraction (SAD) pattern in the inset. Grain size of ~150 nm was visible in several areas of individual wire. Some of the metal grains were found to be faceted at E in Fig. 4(a) that extends across the diameter of the wire. The SAD pattern showed in the inset of Fig. 4(a) confirmed the nanowires to be Ni. The (111) and (200) spacings of fcc Ni were marked at Y and Z, respectively. Figure 4(b) shows the dark field TEM image of a coarse Ni grain that has reasonably high density of fine dislocations. The reflections in the diffraction pattern are for (111) Ni spacings. From histogram analysis, the mean diameter was measured at around 108 nm. Figure 4(c) shows the bright field image of nickel nanowires fabricated at a deposition temperature of 60 °C. To delineate the inherent morphology of each individual nanowire, the cross sections were obtained by FIB milling from the middle of the wires. It is surprising to note that higher deposition temperature resulted in ultrafine grain structure with size of maximum number of grains ~10 nm. This necessarily means self-similar fractal growths observed in SEM images were mainly composed of nanogranules, formed by the random walk of depositing ion as evidenced in the case of other diffusion limited aggregation processes.[13,14]

B. X-ray diffraction

XRD analysis confirmed the polycrystalline nature of the nickel electrodeposits. Figures 5(a)–5(c) showed XRD pattern of the nickel nanowires inside NCA having different nominal pore diameters. Figure 3(d) shows the XRD pattern of the nickel nanowires deposited in NCA200 at lower deposition temperature (40 °C). The comparison between Figs. 5(a) and 5(d) revealed that when deposition occurred from an electrolyte having solution temperature of 60 °C, the orientation showed the peak intensities as (111)>(200)>(220)>(311)>(222). Deposition from a lower bath temperature (40 °C) showed an orientation as (111)>(220)>(200)>(311)>(222). The wires deposited at 40 °C showed a stronger (220) preferred orientation as opposed to (200) at 60 °C. Since the (220) crystal orientation was in the direction of wire growth during deposition and the (200) orientation lied in perpendicular direction to the wire axis,[15] for NCA20, most of the crystals were oriented in the (220) orientation due to the constrain in total area for nucleation imposed by small pore diameters in the [200] direction.

Scherrer formula was employed to calculate the grain size of the nickel electrodeposits. Peak broadening due to the instrument was taken into consideration and ceria (CeO_2) standard sample was used to substract the error due to instrumental broadening. Low temperature samples showed a grain size of 112 nm, whereas high temperature samples

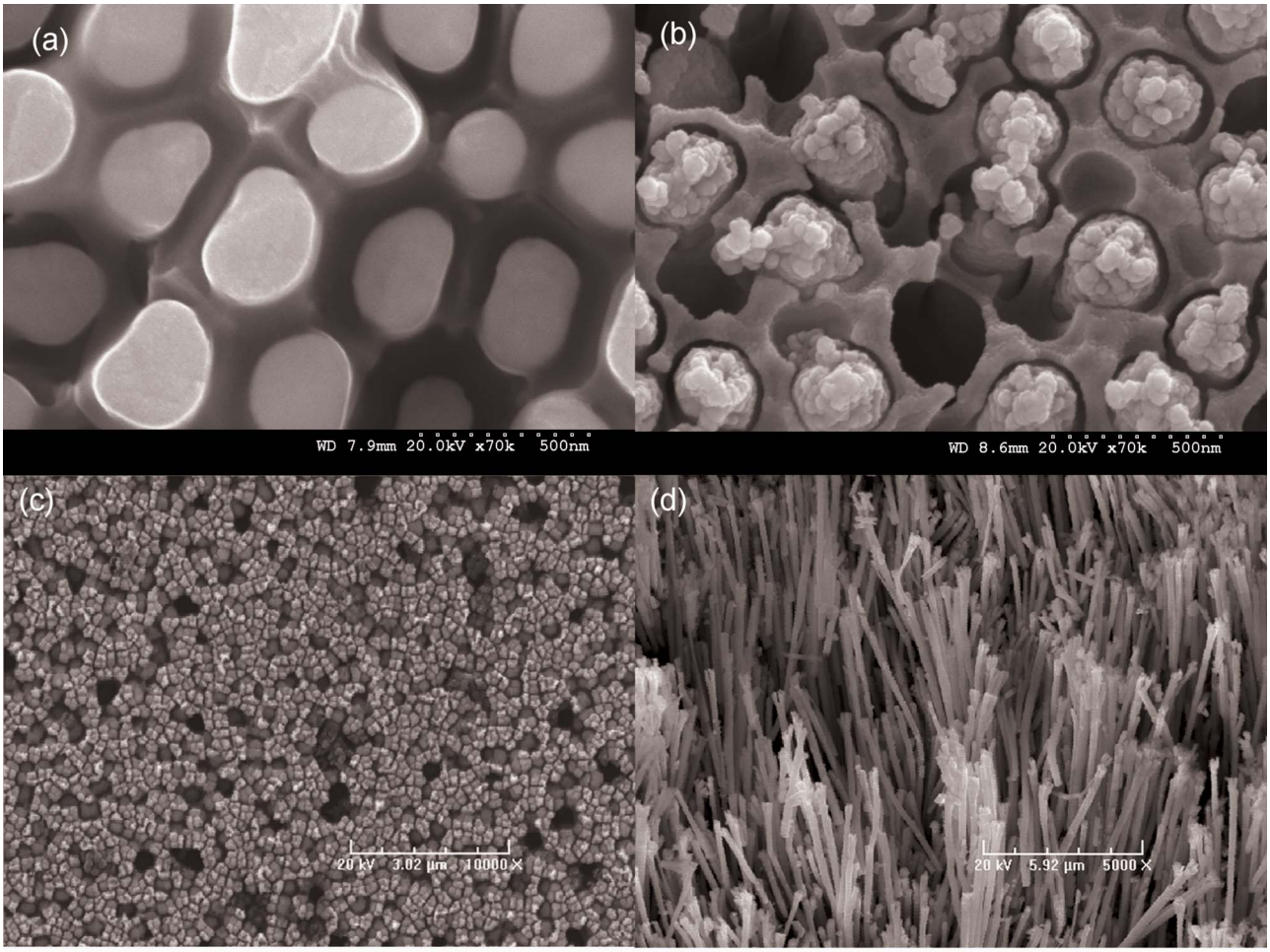


FIG. 3. (a) SEM of top of the nickel nanowires deposited at 40 °C in NCA200 template where the wires came out of the pores. (b) Nickel nanowire deposited at 60 °C. (c) Micrograph showing seed-layer side of the "low temperature" sample after removing Al substrate. (d) Branching of nanowires after completely removing alumina.

showed 33 nm average grain size, which are comparable to the average grain sizes obtained from TEM study.

C. Thermal diffusivity measurements

To evaluate the thermal diffusivity property of nickel nanowires, the NCA templates were first characterized. A 500 nm Al layer was sputtered on the templates. Thermal diffusivity measurement was carried out along the pores of the NCA, with and without Ni nanowires. To calibrate the setup, samples of known thermal diffusivity such as aluminium and nickel were measured. The measured diffusivity values were in good agreement with values obtained from literature.[16] The details of the experimental thermal diffusivity values are reported in Table I.

Figure 6 shows the normalized thermal signal curves of NCA200, NCA100, and NCA20 templates without carbon black, where the transients shifted toward right in the logarithmic time scale with decreasing pore diameters. This attributed to decreasing thermal diffusivity for decreasing pore diameters, i.e., porosity of templates. The preamplifier output, which depicted the intensity of the thermal signal, is also decreasing with decreasing porosity. Air has higher thermal diffusivity than alumina and, therefore, in the case of higher porosity template such as NCA200, it can be assumed that 50% of heat signal reached the other side of the template sooner than the signal traveling through alumina. As a result, some measurements showed double peaks, specifically when the thermal transients were recorded for a small time scale (<1 ms), as can be observed in the inset of Fig. 6. Hence, the templates were measured after spraying the top surface with carbon black. The reported thermal diffusivity of carbon layer is $(1.5 \pm 0.5) \times 10^{-6}$ m^2 s^{-1}, similar to the thermal diffusivity of NCA itself and, therefore, should have minute effect. The thermal diffusivity of NCA20 templates was found to be 1×10^{-6} m^2 s^{-1} at 300 K, which is the same value reported by Borca-Tasciuc and Chen, measured by photothermoelectric technique.[17] To avoid error in the thickness measurements, squared as in Eq. (2), the sample thicknesses were measured from the cross sections by using scanning electron micrograph. The thickness of the samples was usually the thickness of the NCA templates, which is 62 ± 2 μm.

The typical thermal transients for nickel nanowires embedded inside three different templates, fabricated at 40 °C, are shown in Fig. 7. The thermal diffusivity values of NCA without nickel nanowires and Ni-NCA composites fabricated at different temperatures are reported in Table II. All composite samples showed a higher thermal diffusivity than

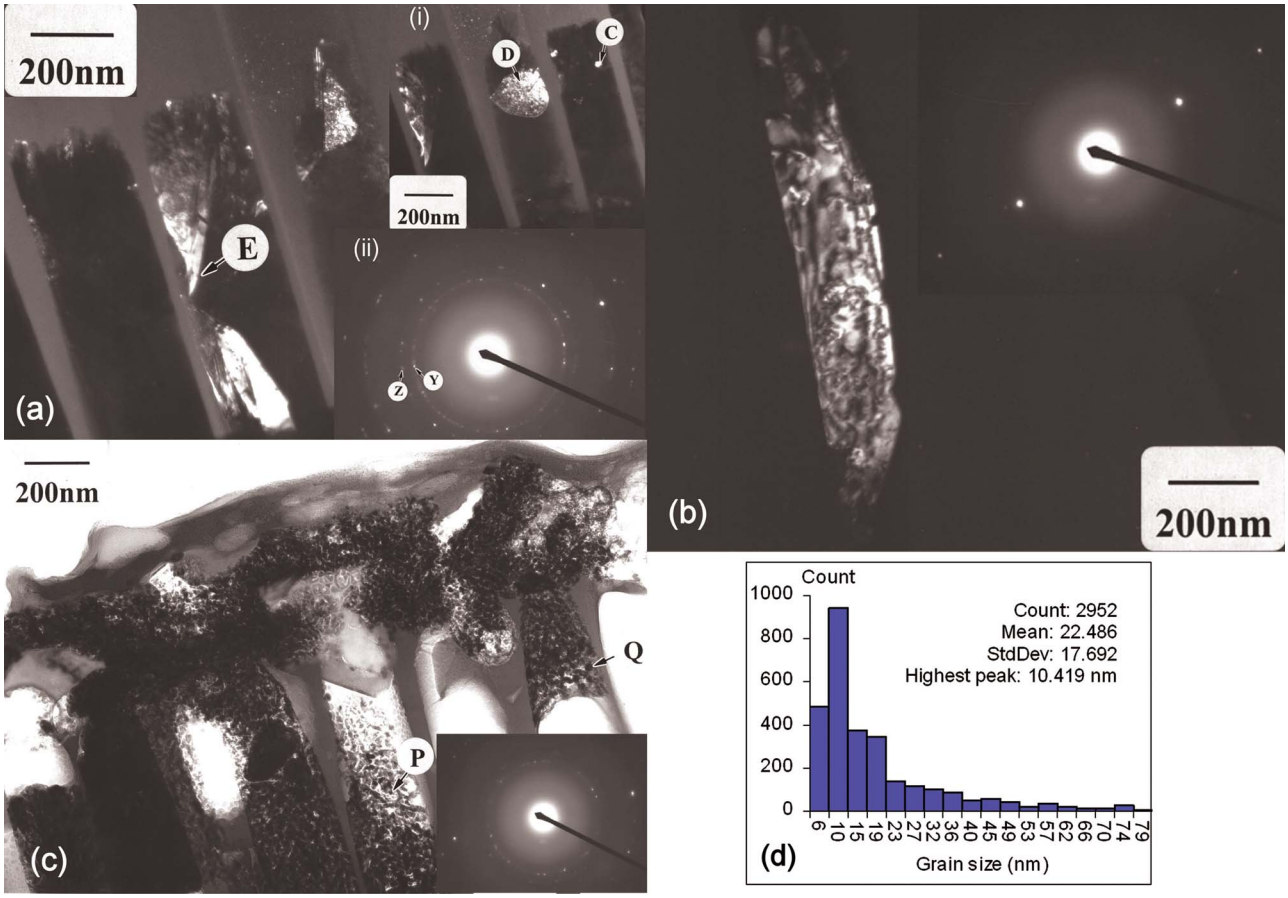


FIG. 4. (Color online) (a) Dark field TEM image showing large faceted grains for nanowires deposited at 40 °C. Insets: (i) shows spherical grains at "D;" (ii) SAD pattern reveals the polycrystalline nature of nickel, showing (111) and (200) spacings. (b) Single crystal grain showing high density of fine dislocations and the corresponding SAD pattern. (c) Bright field TEM image of Ni nanowires deposited at 60 °C showing fine grain structures and the corresponding SAD pattern (inset). (d) Grain size histogram analysis of 60 °C sample.

NCA templates, which was due to a higher diffusivity of nickel. Comparison among nickel-NCA composites showed increasing diffusivity values of 6.5×10^{-6}, 8.5×10^{-6}, and 10.7×10^{-6} m^2 s^{-1}, when the porosity (i.e., pore diameter) of the templates was increasing for low temperature samples. A similar trend was observed in high temperature samples. With increasing porosity of templates, nickel content in the samples is also increasing, and thereby, thermal diffusivity increased. One of the interesting outcomes of the diffusivity measurements was that the low temperature sample showed a higher diffusivity value than the high temperature one having similar pore diameter.

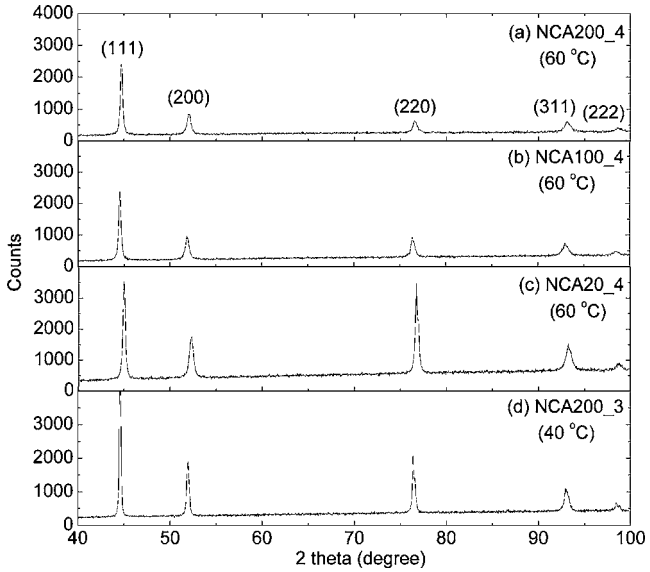


FIG. 5. X-ray diffraction of nickel nanowires showed polycrystalline growth deposited at 60 °C in (a) NCA200, (b) NCA100, and (c) NCA20. (d) shows the XRD pattern for NCA200 sample fabricated at a temperature of 40 °C.

Figure 8 shows the experimental thermal diffusivity values as a function of Ni percentage present in the nickel-NCA composites for both 40 and 60 °C samples. The diffusivity values of NCA templates were also inserted for comparison. MEMT for aligned continuous fibers was employed to calculate the thermal diffusivity according to Eq. (4). Considering the bulk thermal conductivity of alumina (1.9 W m^{-1} K^{-1}) and Ni (90.7 W m^{-1} K^{-1}), the calculated

TABLE I. Thermal diffusivity of Ni and Al foil measured at $10T_{0.5}$ ($\times10^{-6}$ m^2 s^{-1}) by using the laser flash technique compared with reference values.

Samples	Reference 16	Measured
Nickel foil	22.95	22.7
Aluminum foil	95.38	94.7

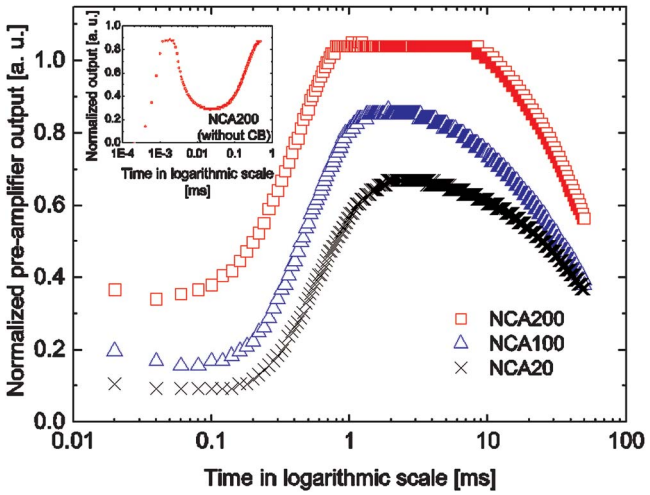


FIG. 6. (Color online) Thermal transients of templates NCA200, NCA100, and NCA20 with Al seed layer.

values overestimated the experimental data for both sets of samples. If the thermal conductivity of nickel nanowires reduced to 78% of the bulk value, then Eq. (4) could predict the experimental results of low temperature samples. In this case, nickel nanowires have an effective thermal conductivity of 70.7 W m^{-1} K^{-1}. High temperature experimental data fit well with the theoretical prediction when thermal conductivity of Ni was reduced to 40% of the bulk value, resulting in an effective conductivity of 36.28 W m^{-1} K^{-1}.

To examine the effect of electrodeposition temperature, we referred back to the XRD and TEM analysis of the grains. For 40 °C samples, the average grain size was 112 nm, whereas for 60 °C samples, it was 34 nm according to the XRD peak analysis. TEM observation revealed that the low temperature samples have grains (150 nm) that extend across the pore diameter. For large grain size (i.e., low temperature samples), the reduction in conductivity we observed is believed to arise from the inherent defects, i.e., dislocations in the grain crystal structure, as evident in Fig. 4(b), and reduction of the wire diameter according to the corresponding

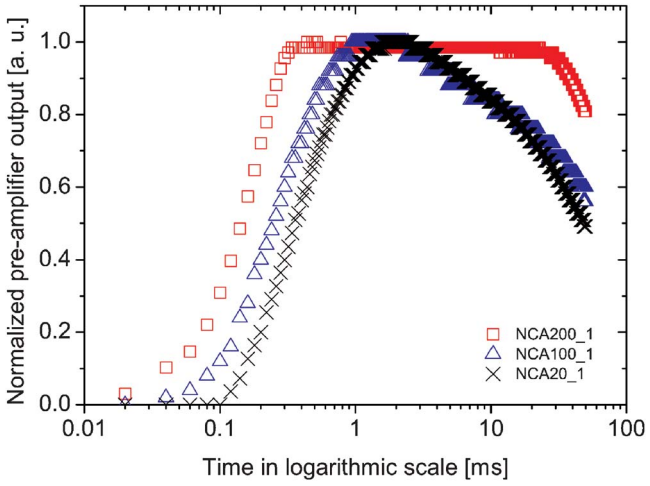


FIG. 7. (Color online) Thermal transients of nickel nanowires embedded inside NCA200, NCA100 and NCA20, templates, fabricated at 40 °C with a current density of 10 mA cm^{-2}.

TABLE II. Thermal diffusivity of NCA templates measured at $10T_{0.5}$ ($\times 10^{-6}$ m^2 s^{-1}) before and after growth of Ni nanowires fabricated at different temperatures.

	NCA200	NCA100	NCA20
Temp. (°C)	2.0 NCA200_Ni	1.4 NCA100_Ni	1.0 NCA20_Ni
40	10.7	8.5	6.5
60	5.6	4.9	3.6

NCA. On the other hand, in high temperature samples, each individual nanowire had fractal morphology in macroscale, which further consists of nanogranules. The size of maximum number of grains is found to be ~10.4 nm, which is comparable to electron mean free path (~5.7 nm) of nickel. Thermal transport in nickel is dominated by electron heat transfer mechanism where phonon contribution is around 8.5%.[18] The reduction in size of the grains to nanometric dimension leads to tremendous increase in interfacial area compared to large grain low temperature samples. This will lead to manifold increase in grain boundary scattering of conduction electrons as well as phonons, which, in turn, decreases the overall thermal conductivity of the wires. Moreover, for the size of most of the grains being comparable to electron mean free path, there will be a low cutoff frequency of lattice vibration modes, which is known as softening of phonon spectrum. This will lead to further reduction in conductivity. It was interesting to note that a recent theoretical study on Ni nanoparticles showed an overall thermal conductivity of 36.4 W m^{-1} K^{-1} for particle size of 10.56 nm, which corroborates our experimental observation.[18]

VI. CONCLUSIONS

In summary, we have fabricated the nickel nanowire-alumina composites, where the grain growth was tuned by deposition temperature. The diameter of nanowires and nickel content in NCA are directly related to the pore diameter and porosity of the templates. The crystal orientation can be controlled as well by varying the pore diameter and the

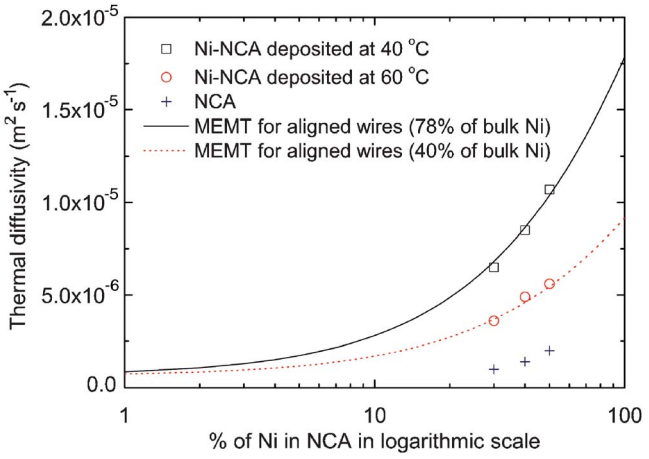


FIG. 8. (Color online) Thermal diffusivity with respect to %Ni in NCA at different temperatures. Solid curve: MEMT (78% of bulk conductivity of Ni). Dotted curve: MEMT (40% of bulk conductivity of Ni).

deposition temperature. The thermal diffusivity data for nanowire-alumina composites showed grain size dependence. MEMT model for aligned fibers adeptly described the experimental values. A strong grain size dependence of thermal diffusivity in the nanowires was observed. It is believed that the decrease in diffusivity in lower temperature wires is associated with defects/dislocations in large single crystals and reduction in wire diameters according to the pore diameter of NCA. Whereas in higher temperature wires, the drastic reduction in diffusivity is believed to arise from self-similar fractal morphology composed of nanogranules, close to the dimension of electron mean free path.

ACKNOWLEDGMENTS

This work is financially supported by Enterprise Ireland (EI) under the Industry Led Research Programme (No. ILRP/05/PEIG/7) in Power Electronics and Science Foundation Ireland (SFI) Principal Investigator (PI) grant no. 06/IN.1/I98.

[1]R. S. Prasher, P. Koning, J. Shipley, and A. Devpura, J. Electron. Packag. **125**, 386 (2003).
[2]P. K. Schelling, Li Shi, and K. E. Goodson, Mater. Today **8**, 30 (2005).
[3]C. H. Liu, H. Huang, Y. Wu, and S. S. Fan, Appl. Phys. Lett. **84**, 4248 (2004).
[4]T. Borca-Tasciuc, S. Vafaei, D.-A. Borca-Tasciuc, B. Q. Wei, R. Vajtai, and P. M. Ajayan, J. Appl. Phys. **98**, 054309 (2005).
[5]T. Kehoe, Ph. D. thesis, University College Cork, 2006.
[6]L. Kehoe, P. V. Kelly, and G. M. Crean, Microsyst. Technol. **5**, 18 (1998).
[7]W. J. Parker, R. Jenkins, C. P. Butler, and G. L. Abbot, J. Appl. Phys. **32**, 1679 (1961).
[8]D. P. Almond and P. M. Patel, *Photothermal Science and Techniques*, (1st ed. Chapman and Hall, London, 1996), p. 211.
[9]R. D. Cowan, J. Appl. Phys. **34**, 926 (1963).
[10]C.-W. Nan, R. Birringer, D. R. Clarke, and H. Gleiter, J. Appl. Phys. **81**, 6692 (1997).
[11]D.-A. Borca-Tasciuc, G. Chen, A. Prieto, M. S. Martín-González, A. Stacy, T. Sands, M. A. Ryan, and J. P. Fleurial, Appl. Phys. Lett. **85**, 6001 (2004).
[12]K. M. Razeeb, Ph. D. thesis, University of Limerick, 2003.
[13]S. Roy and D. Chakravorty, Appl. Phys. Lett. **59**, 1415 (1991).
[14]S. Roy and D. Chakravorty, Phys. Rev. B **47**, 3089 (1993).
[15]I. Z. Rahman, K. M. Razeeb, M. A. Rahman, and Md. Kamruzzaman, J. Magn. Magn. Mater. **262**, 166 (2003).
[16]*CRC Handbook of Chemistry and Physics*, edited by R. C. Weast (CRC, Florida, 1994).
[17]D.-A. Borca-Tasciuc and G. Chen, J. Appl. Phys. **97**, 084303 (2005).
[18]S. P. Yuan and P. X. Jiang, Int. J. Thermophys. **27**, 581 (2006).